Sixth International Symposium on Turbulence and Shear Flow Phenomena
Seoul, Korea, 22-24 June 2009

IMPLICIT LARGE EDDY SIMULATION OF FLOWS AROUND BODIES OF ARBITRARY SHAPE ON CARTESIAN GRIDS USING A CONSERVATIVE IMMERSED INTERFACE METHOD

M. Meyer, A. Devesa, S. Hickel, X.Y. Hu, N.A. Adams
Technische Universität München,
Institute of Aerodynamics,
85747 Garching, Germany
corresponding author: michael.meyer@aer.mw.tum.de

ABSTRACT

This work presents an immersed interface method for representing complex boundaries in Implicit Large-Eddy Simulation on three-dimensional, staggered Cartesian Grids.

The immersed obstacle in the fluid domain is characterized by a levelset field. Initial flux calculations are carried out for the entire domain in the same way. Cells intersected by the immersed interface then undergo a special treatment: only the fluid part is considered, no-slip condition and no-through-flux condition are imposed by changing the flux balance and a homogeneous Neumann condition for pressure is enforced in the pressure projection. To deal with the small cell problem a cell-mixing procedure is applied. The approach is fully conservative and we demonstrate the method is second-order accurate.

The validation and the performance of the approach are done with some numerical examples of 2D and 3D flow configurations.

INTRODUCTION

Implicit Large Eddy Simulation (ILES) has shown considerable potential for the efficient representation of physically complex flows, see e.g. Hickel and Adams (2008). In ILES the truncation error of the discretization of the convective terms acts as a subgrid-scale model which is therefore implicit to the discretization. In this context, the Adaptive Local Deconvolution Method (ALDM) (Hickel et al., 2006a; Hickel and Adams, 2006b) uses a discretization based on solution-adaptive deconvolution which allows to control the nonlinear truncation error. Deconvolution parameters are determined by an analysis of the spectral numerical viscosity. ALDM is incorporated into a finite volume numerical solver for the incompressible Navier-Stokes equations discretized on a staggered grid. Applications to generic configurations, such as isotropic turbulence (Hickel and Adams, 2006a), plane channel flow (Hickel and Adams, 2007), and turbulent boundary layer separation (Hickel and Adams, 2008) show excellent agreement with the corresponding results from theory, experiment, or direct numerical simulations. Given this performance the motivation is to use ALDM for the investigation of complex flow configurations of practical relevance. As ILES employs the truncation error as subgrid scale model, one has to take into account the grid-dependence of the truncation error. Although ALDM has been successfully formulated for and implemented also into a curvi-linear flow simulation code, a purely Cartesian-mesh formulation has conceptual and computational advantages.

Usually, the generation of good-quality body-fitted grids can be time-consuming and difficult. Contradictory requirements, namely adequate local resolution and minimum number of grid points, can deteriorate the grid quality and therefore adversely affect accuracy and numerical convergence properties. Alternatively, the discretization of the domain can be performed on a Cartesian mesh. Cartesian meshes also imply fewer computational operations per grid point. Bounding surfaces of the flow can be accounted for by an Immersed Boundary (IB) approach. An overview on existing approaches is given in by Mittal and Iaccarino (2005), for which discrete mass and momentum conservation and high-order accuracy near the interfaces pose a challenge. Accurate representation of the flow near the boundaries, however, is essential for LES of wall-bounded turbulence. The method proposed in this paper is second-order accurate and ensures mass as well as momentum conservation.

In section *Conservative Immersed Interface Method* a description of the different steps for imposing the immersed boundary condition is given. Validation results for laminar flow around square and round cylinders at Re = 100 and turbulent flow around a round cylinder at Re=3,900 are presented in section *Numerical examples*, followed by a *Conclusion*.

CONSERVATIVE IMMERSED INTERFACE METHOD

Our approach consists of two parts: a standard procedure applied to all cells of the entire computational domain and a special procedure for the cut cells. As standard procedure the following finite volume discretization of the incompressible governing equations is used

$$\begin{aligned}\mathbf{u}^{\mathbf{n+1}}_{\mathbf{i,j,k}} V_{i,j,k} = \mathbf{u}^{\mathbf{n}}_{\mathbf{i,j,k}} V_{i,j,k} \\ +\triangle t \left[S_{i+1/2,j,k} \mathbf{F}_{i+1/2,j,k} - S_{i-1/2,j,k} \mathbf{F}_{i-1/2,j,k} \right] \\ +\triangle t \left[S_{i,j+1/2,k} \mathbf{F}_{i,j+1/2,k} - S_{i,j-1/2,k} \mathbf{F}_{i,j-1/2,k} \right] \\ +\triangle t \left[S_{i,j,k+1/2} \mathbf{F}_{i,j,k+1/2} - S_{i,j,k-1/2} \mathbf{F}_{i,j,k-1/2} \right]\end{aligned} \tag{1}$$

where $\mathbf{u} = [u, v, w]$ represents the velocity in the cell (i,j,k) which is integrated over its cell volume $V_{i,j,k}$. The superscripts n and $n+1$ indicate the time step. $\mathbf{F}_{i\pm1/2,j,k}$, $\mathbf{F}_{i,j\pm1/2,k}$, $\mathbf{F}_{i,j,k\pm1/2}$ are the fluxes over the corresponding cell faces S integrated in time with Δt thanks to an explicit first-order time difference. The flux formulation above also

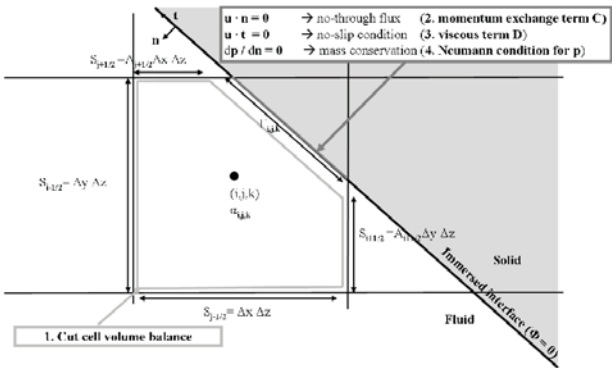

Figure 1: Overview on the different steps of the conservative immersed interface method with regard to a cut cell (i,j,k)

contains the convective fluxes which discretization error is designed to function as Subgrid Scale Model in ALDM. For details on ALDM, the reader is referred to the papers by Hickel and co-authors (2006a, 2006b, 2007).

Cut-cell volume balance

The immersed obstacle in the fluid domain is characterized by a levelset field Φ, i.e. a signed distance function for each point of the domain with respect to the immersed surface. The zero-levelset contour ($\Phi = 0$) describes the interface between the fluid and the obstacle. The intersection between the immersed boundary and the finite volume cell is assumed to generate a linear interface separating fluid and solid part (see Fig. 1). The volume fraction of the fluid part is denoted $\alpha_{i,j,k}$ and is such as $0 \leq \alpha_{i,j,k} \leq 1$. Respectively, the volume $V_{i,j,k}$ can now be expressed as $V_{i,j,k} = \alpha_{i,j,k} \triangle x \triangle y \triangle z$. The cell faces S are now represented by two parts: one is the combination of the six segments of cell faces cut by the interface, which can be written in the form of $A_{i\pm1/2,j,k} \triangle y \triangle z$, $A_{i,j\pm1/2,k} \triangle x \triangle z$, and $A_{i,j,k\pm1/2} \triangle x \triangle y$, where $1 \leq A \leq 0$ is the face aperture, the other is the surface of the interface $\Gamma_{i,j,k}$ itself inside of the cell (i,j,k). For a cut cell the general formulation of Eq. 1 yields

$$\begin{aligned}\mathbf{u^{n+1}_{i,j,k}} = \mathbf{u^{n}_{i,j,k}} &+ \frac{\triangle t \left[A_{i+1/2,j,k}\mathbf{F}_{i+1/2,j,k} - A_{i-1/2,j,k}\mathbf{F}_{i-1/2,j,k}\right]}{\alpha_{i,j,k}\triangle x} \\ &+ \frac{\triangle t \left[A_{i,j+1/2,k}\mathbf{F}_{i,j+1/2,k} - A_{i,j-1/2,k}\mathbf{F}_{i,j-1/2,k}\right]}{\alpha_{i,j,k}\triangle y} \\ &+ \frac{\triangle t \left[A_{i,j,k+1/2}\mathbf{F}_{i,j,k+1/2} - A_{i,j,k-1/2}\mathbf{F}_{i,j,k-1/2}\right]}{\alpha_{i,j,k}\triangle z} \\ &+ \frac{\triangle t \ (\mathbf{C} + \mathbf{D})}{\alpha_{i,j,k}\triangle x \triangle y \triangle z} \end{aligned} \quad (2)$$

where $\mathbf{C}$ and $\mathbf{D}$ are additional terms to account for the influence of the immersed boundary on the fluid. The meaning of these terms and a sketch of the method is given in Fig. 1. Explanations will follow in the subsections.

Momentum exchange term C

As no fluid should enter the or leave the domain through the obstacle, it must be ensured that the normal velocity is zero at the interface. This is achieved with a momentum exchange approach, which adds an unphysical convective term $\mathbf{C}$ to the flux balance. For cells with a volume fraction $\alpha_{i,j,k} \leq 0.5$ we impose the zero normal velocity with a velocity projection. We determine the wall-normal velocity $\mathbf{u}_{C,i,j,k,\perp} = -\mathbf{u}_{i,j,k,\perp}$ for (i,j,k). As this is a time independent and volume-independent boundary condition we have to compensate the time integration from Eq. 2 by a division with $\triangle t$ and the volume integration by devision with the real cell volume.

$$\mathbf{C} = -\mathbf{u}_{C,i,j,k,\perp} \frac{\alpha_{i,j,k}\triangle x \triangle y \triangle z}{\triangle t} \quad (3)$$

With this formulation we directly impose zero normal velocity. $\mathbf{C}$ is added to the flux balance.

Friction term D

A fluid moving along a solid boundary exerts a shear stress on that boundary due to the no-slip condition. For meshes aligned with the boundary, such as body-fitted structured meshes, the imposition of the no-slip condition is straightforward. In order to account for the shear stress due to the immersed boundary on a Cartesian mesh, we add a friction force to the flux balance of the cut cell (see Fig. 1). For a non-moving wall, this term can be expressed as

$$\mathbf{D} = -\int_\Gamma \boldsymbol{\tau}_{wall}\mathbf{n}dS = -\int_\Gamma \mu \frac{\partial \mathbf{u}}{\partial n} dS = -\mu\Gamma_{i,j,k}\frac{\mathbf{u}_\parallel - \mathbf{u}_{\mathbf{BC},\parallel}}{h_{i,j,k}} \quad (4)$$

$$h_{i,j,k} = \frac{\sqrt{h_i^2 + h_j^2 + h_k^2}}{2} \quad (5)$$

In accordance with the finite volume dicretization the shear stress τ_{wall} is integrated over the fluid-solid interface Γ. $\partial u / \partial n$ only considers the tangential velocity. μ represents the dynamic viscosity. In order to approximate the velocity difference, we use the difference of the tangential velocity and the velocity at the boundary $\mathbf{u}_{\mathbf{BC},\parallel}$. As geometric derivative the characteristic length of the cell $h_{i,j,k}$ is taken. The negative sign is due the immersed boundary influencing the fluid and not the opposite.

Homogeneous Neumann condition for pressure

For solving the elliptic Poisson equation we impose a homogeneous Neumann condition at the immersed interface (see Fig. 2). The discretized Poisson equation can be written as

$$\begin{aligned}\nabla^2 p = &+ \frac{\left[A_{i+1/2,j,k}\ u_{i+1/2,j,k} - A_{i-1/2,j,k}\ u_{i-1/2,j,k}\right]}{\alpha_{i,j,k}\triangle x} \\ &+ \frac{\left[A_{i,j+1/2,k}\ v_{i,j+1/2,k} - A_{i,j-1/2,k}\ v_{i,j-1/2,k}\right]}{\alpha_{i,j,k}\triangle y} \\ &+ \frac{\left[A_{i,j,k+1/2}\ w_{i,j,k+1/2} - A_{i,j,k-1/2}\ w_{i,j,k-1/2}\right]}{\alpha_{i,j,k}\triangle z} \\ &- \frac{\Gamma_{i,j,k}\ r^i_{i,j,k}}{\Delta x\ \Delta y\ \Delta z\ \alpha_{i,j,k}} \end{aligned} \quad (6)$$

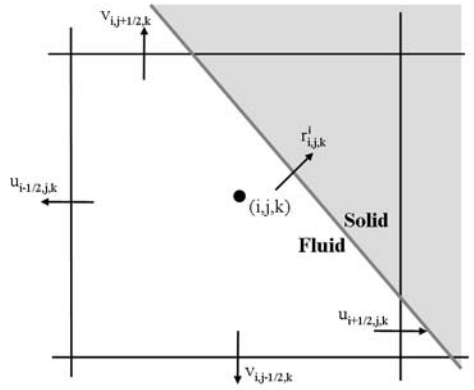

Figure 2: Fluxes of the discretized pressure-Poisson equation of a cut cell (i,j,k)

where u, v, w are the velocities at the cell faces and $r^i_{i,j,k}$ is the interface condition for the pressure of the cut cell i,j,k. We set the $r^i_{i,j,k}$ to zero, which is equivalent to imposing the homogeneous Neumann condition $\partial p/\partial n = 0$ on the interface.

Mixing procedure

Cartesian cut cell methods, such as the one presented in this paper, inevitably generate small fluid cells. A special treatment of these cells is mandatory since a stable fluid state may not be obtained based on the time step calculated according to the full grid size CFL condition.

In the presented method, the fluid of the small cells is mixed with that of the neighboring cells. As a basis, the approach of Hu et al. (2006) is considered and formulated on staggered grids and in three dimensions. In our case small cells are those with a volume fraction $\alpha_{i,j,k} \leq 0.5$. Targeted cells are determined from an evaluation of the normal vector of the quadratic surfaces, as shown in Fig. 3. The changes of the conservative quantities in the x and y direction for the small cell (i,j,k) and their targeted cells in x, y and z direction are calculated by

$$\mathbf{M}^x = \frac{\beta^x_{i,j,k}}{\beta^x_{i,j,k}\alpha_{i,j,k} + \alpha_{tgt}} [\alpha_{i,j,k}(\alpha\mathbf{u})_{tgt} - \alpha_{tgt}(\alpha\mathbf{u})_{i,j,k}] \quad (7)$$

$$\mathbf{M}^y = \frac{\beta^y_{i,j,k}}{\beta^y_{i,j,k}\alpha_{i,j,k} + \alpha_{tgt}} [\alpha_{i,j,k}(\alpha\mathbf{u})_{tgt} - \alpha_{tgt}(\alpha\mathbf{u})_{i,j,k}] \quad (8)$$

$$\mathbf{M}^z = \frac{\beta^z_{i,j,k}}{\beta^z_{i,j,k}\alpha_{i,j,k} + \alpha_{tgt}} [\alpha_{i,j,k}(\alpha\mathbf{u})_{tgt} - \alpha_{tgt}(\alpha\mathbf{u})_{i,j,k}] \quad (9)$$

where tgt is the indice of the target cell. The terms $\beta^x_{i,j,k}$, $\beta^y_{i,j,k}$ and $\beta^z_{i,j,k}$ are the fractions of mixing in the x, y and z directions respectively and satisfy $\beta^x_{i,j,k} + \beta^y_{i,j,k} + \beta^z_{i,j,k} = 1$. Note that conservation is ensured since the conservative quantities that a small cell obtained from a target cell $M_{i,j,k}$, corresponds to a loss of the target cell M_{tgt}.

$$\mathbf{M}^x = \mathbf{M}^x_{i,j,k} = -\mathbf{M}^x_{tgt} \quad (10)$$

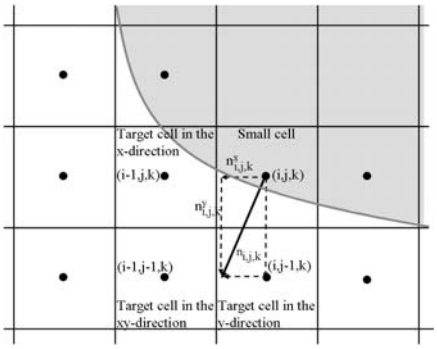

Figure 3: Mixing procedure for a small cell (i,j,k)

$$\mathbf{M}^y = \mathbf{M}^y_{i,j,k} = -\mathbf{M}^y_{tgt} \quad (11)$$

$$\mathbf{M}^z = \mathbf{M}^z_{i,j,k} = -\mathbf{M}^z_{tgt} \quad (12)$$

In our approach we also consider diagonal cells, so that we have three target cells in two dimensions, and seven target cells in three dimensions. Once the mixing changes are determined for all small cells the conservative quantities of the near-wall cells are updated by

$$(\alpha\mathbf{u})^{n+1}_{i,j,k} = (\alpha\mathbf{u})^{n+1\star}_{i,j,k} + \sum_k \mathbf{M}^x + \sum_l \mathbf{M}^y + ... + \sum_o \mathbf{M}^{xyz} \quad (13)$$

where $(\alpha\mathbf{u})^{n+1\star}_{i,j,k}$ are the conservative quantities before mixing to which the summations taken for all the mixing operations in the different directions are added. The approach does not only hold for mixing velocity but also for scalar concentration. Since it is carried out before the pressure projection, the solution after each time step is divergence free.

NUMERICAL EXAMPLES

The computational domain for the following numerical examples is shown in Fig. 4. The upper and lower boundaries are characterized by free-slip boundary conditions. In spanwise direction periodic boundary conditions are imposed. At the inlet a uniform velocity and at the outlet a pressure condition is defined. On the boundary of the obstacle the immersed interface condition is imposed by the presented Conservative Immersed Interface Method (CIIM).

For the discretziation in space ALDM is used for the convective terms, and a second order accurate Central Difference Scheme (CDS) for the diffusive terms. Time advancement is performed using a third order three step Runge-Kutta scheme. The Poisson equation is solved using Bi-Conjugate Gradient Stabilized (BiCGStab) iterative solver. All computations are carried out with a CFL number of 0.5. The Reynolds number in the different configuration cases is always given with regard to the diameter d, the freestream viscosity ν_∞ and freestream velocity u_∞.

Flow past a square cylinder at Re = 100

At this Reynolds number the flow is found to be two-dimensional and laminar. The points of separation are fixed

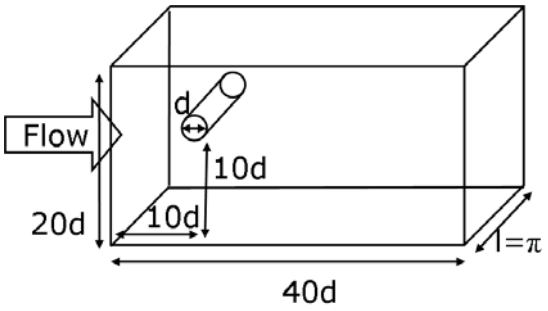

Figure 4: Computational domain for numerical examples

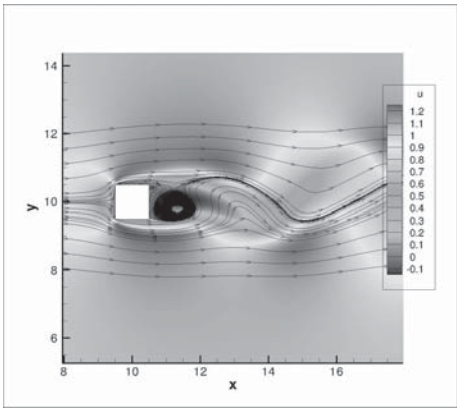

Figure 5: U-velocity and streamlines for flow past a square cylinder at $Re = 100$

Table 1: Results for flow past a square cylinder at $Re = 100$

Case	C_D	C_L	St
Okajima, 1982	-	-	0.149
Davis and Moore, 1982	1.63	-	0.152
Franke et. al, 1990	1.61	0.27	0.154
Present (Fine grid: 76pts/d)	1.57	0.27	0.151

at the sharp rear corners of the cylinder. The wake shown (see Fig. 5) was found to be unsteady with vortex shedding at a Strouhal number $St = 0.151$, which agrees well with the experiments.

The Strouhal number, the drag coefficient C_D and the lift coefficient C_L of our calculation are compared to the ones from the literature in Table 1. The lift coefficient agrees very well with the simulation by Franke et al. (1990). The drag coefficient of our calculation is slightly lower than the value obtained by Franke. However, due to numerical and experimental uncertainties related to the sharp corners of this configuration case, discrepancies in the obtained values are commonly expected.

To determine the convergence order of the CIIM, the drag and lift coefficient calculations have been performed on five grids with different resolution. All grids have been stretched according to a tangent hyperbolic function with a ratio of -1.5 around the xz-, yz- symmetry planes of the cylinder. The grids are summarized in Table 2.

Table 2: Grids for flow past a square cylinder at $Re = 100$

Grid	Nbr of pts domain	Nbr of pts per d
A	128 x 64	15
B	192 x 96	23
C	256 x 128	34
D	384 x 192	51
E	512 x 256	76

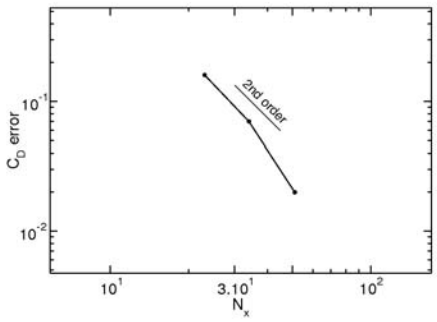

Figure 6: Error in C_D for flow past a square cylinder at $Re = 100$ calculated on different grids

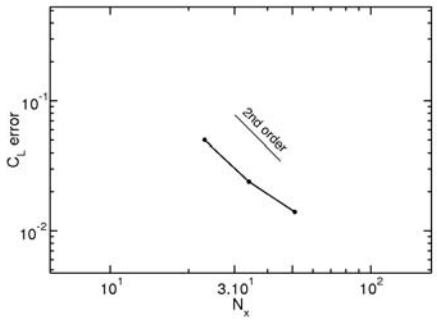

Figure 7: Error in C_L for flow past a square cylinder at $Re = 100$ calculated on different grids

The error is calculated with respect to the solution on the finest grid. In Fig. 6 and Fig. 7 we show a log-log plot of the errors for C_D and C_L. Also shown is a line with a slope of -2 which corresponds to a second-order convergence rate. The plot shows that the error decreases in a manner consistent with a second-order accurate scheme.

Flow past a round cylinder at Re = 100

At this Reynolds number the flow around a circular cylinder behaves in a very similar way to the flow around a square cylinder. The flow is two-dimensional and laminar. The main difference is the fact that the points of separation are not fixed at any sharp corners of the cylinder. In good agreement with the literature, flow separation occurs at the rear part of the cylinder at a separation angle of $\Phi = 118°$ (see also Fig. 8). The vortices are approximately half the size of the ones appearing in the square cylinder case, while not reaching over the middle plane of the cylinder. For the unsteady

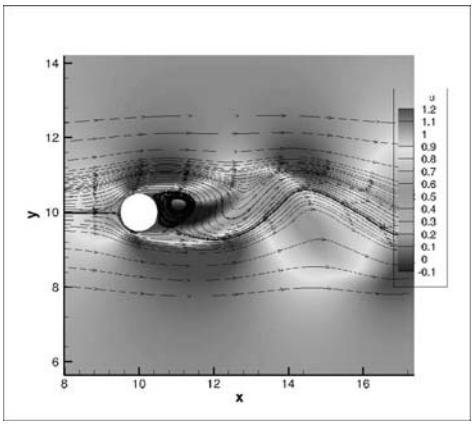

Figure 8: U-velocity and streamlines for flow past a round cylinder at $Re = 100$

Table 3: Results for flow past a round cylinder at $Re = 100$

Case	C_D	C_L	St	St
Tritton, 1959	1.3	-	-	-
Henderson, 1995	1.3	-	-	-
Fey et. al, 1998	-	-	0.165	-
Kim et. al, 2001	1.33	0.32	0.165	-
Dröge, 2007	1.24	0.33	0.165	-
Present (Fine grid: 76pts/d)	1.30	0.33	0.165	-

Table 4: Grids for flow past a round cylinder at $Re = 100$

Grid	Nbr of pts domain	Nbr of pts per d
A	128 x 64	15
B	192 x 96	23
C	256 x 128	34
D	384 x 192	51
D	512 x 256	76

wake, vortex shedding occurs at St=0.165 which agrees well with the literature.

A comparison of the global quantities St, C_D, C_L obtained from our calculation and those of experimental and numerical results in the literature are summarized in Table 3. Similar to the square cylinder, there is also a dispersion in the results for the circular cylinder. This dispersion certainly traces back to differently predicted flow separation angles which is the crucial parameter for all global quantities. The drag coefficient of our calculation agrees well with those from the experiments (Tritton, 1959; Henderson, 1995) and lays between the values obtained with other cut-cell methods by Kim et al. (2001) and Dröge (2007). The lift coefficient is also in the range of the results of other authors's computations. As the Strouhal number is a quite insensitive quantity it is obvious that the experimental and numerical results from the literature do not differ much.

As for the square cylinder configuration, we want to demonstrate that CIIM converges with second order accuracy. Calculations have been again performed on five grids

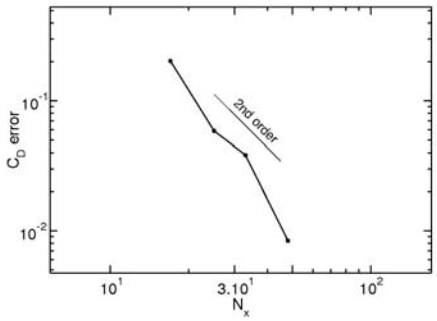

Figure 9: Error in C_D for flow past a round cylinder at $Re = 100$ calculated on different grids

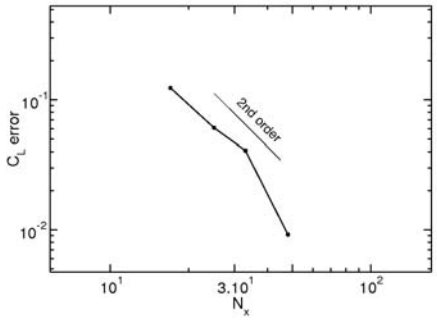

Figure 10: Error in C_L for flow past a round cylinder at $Re = 100$ calculated on different grids

with different resolution. All grids have been stretched according to a tangent hyperbolic function with a ratio of -1.5 around the xz-, yz- symmetry planes of the cylinder. The grids are summarized in Table 4. The order of accuracy is determined for C_D and C_L. The value obtained on the finest grid is taken as reference value for the error calculation . The results are shown in Fig. 9 and Fig. 10. Again the line with a slope of -2 shows that our approach exhibits to second-order accuracy.

Flow past a round cylinder at Re = 3,900

The flow over a round cylinder at $Re = 3,900$ is a much more challenging configuration. The flow is turbulent and thus three-dimensional. Calculations were done on an adaptively refined grid with a total of 7 million cells and at least one computational cell in the viscous sublayer of the cylinder. The resolution of the boundary layer of this flow configuration is important as results are characterized by laminar-turbulent transition of the separated shear layers. Qualitatively good agreement is reached with the results of other calculations: the typical pressure tubes for the p-isosurfaces corresponds with the results reported by Fröhlich (1998). The elongated structures for the x-vorticity shown by Kravchenko (2000) can also be reproduced (Fig. 11). A statistical analysis will be included in the TSFP6 presentation.

Figure 11: x-vorticity-isosurfaces $\pm 1.5^{-1}s^{-2}$ of round cylinder at Re = 3,900.

CONCLUSION

In this paper a new Conservative Immersed Interface Method (CIIM) in the framework of ILES was introduced. According to the Cartesian finite volume approach for ALDM, CIIM operates on fluxes of cut-cells only and therefore ensures mass and momentum conservation. The four major steps to impose the immersed interface condition were briefly explained. As the presented method is constructed based on a standard Cartesian finite volume method and level set technique, it maintains the simplicity of GFM-like methods for implementation and handles topological changes naturally. A number of numerical examples were compared to experiments and Direct Numerical Simulations. The obtained results suggest that the method exhibits second-order convergence and good accuracy. The efficient classification of cut-cells using the Marching Square and Marching Cube approach also allows the extension to multiphase problems and the use of Adaptive Mesh Refinement.

REFERENCES

Davis, R.M., Moore, E.F., 1982, "A numerical study of vortex shedding from rectangles", *Journal of Fluid Mechanics* 116, 475-506

Dröge M. and Verstappen R., 2005, "A new symmetry-preserving Cartesian-grid method for computing flow past arbitrarily shaped objects", *International Journal of Numererical Methods in Fluids* 47, 979985

Fey U. , König M. and Eckelmann H., 1998, "A new Strouhal-Reynolds-number relationship for the circular cylinder in the range $47 < Re < 2 \cdot 10^5$", *Physics of Fluids* 10, 1547

Franke R., Rodi W., Schönung B., 1990, "Numerical Calculation of Laminar Vortex Shedding Flow Past Cylinders", *Journal of Wind Engineering and Industrial Aerodynamics* 35, 237-257

Fröhlich J., Rodi W., Kessler Ph., Parpais S., Bertoglio J.P., and Laurence D., 1998, "Large eddy simulation of flow around circular cylinders on structured and unstructured grids", *CNRS DFG Collaborative Research Programme, Vieweg, Braunschweig* 66, 319338

Henderson R.D., 1995, "Details of the drag curve near the onset of vortex shedding", *Physics of Fluids* 7, 21022104

Hickel S., Adams N.A., 2008, "Implicit LES applied to zero-pressure-gradient and adverse-pressure-gradient boundary-layer turbulence", *International Journal of Heat and Fluid Flow* 29, 626-639

Hickel S., Adams N.A., Domaradzki J.A., 2006a, "An adaptive local deconvolution method for implicit LES", *Journal of Computational Physics* 213, 413-436

Hickel S., Adams N.A., 2006b, "A proposed simplification of the adaptive local deconvolution method", *Proceedings of CEMRACS 2005* ESAIM 16, 66-76

Hickel S., Adams N.A., 2007, "On implicit subgrid-scale modeling in wall-bounded flows", *Physics of Fluids* 19: 105106

Hu X.Y, Khoo B.C., Adams N. A. and Huang F. L., 2006, "A conservative interface method for compressible flows",*Journal of Computational Physics* 219, 553-578

Kim J., Kim D., Choi H., 2001, "An immersed-boundary finite-volume method for simulations of flow in complex geometries", *Journal of Computational Physics* 171, 13250

Kravchenko A. and Moin P., 2000, "Numerical studies of flow over a circular cylinder at $Re_D = 3900$", *Physics of Fluids* 12, 403

Mahesh K. , Constantinescu G. , and Moin P., 2004, "A numerical method for large-eddy simulation in complex geometries",*Journal of Computational Physics*, 197, 215240

Mittal R. , 1996, "Progress on LES of flow past a circular cylinder", *Annual Research Briefs, Center for Turbulence Research, Stanford University*, 233241

Mittal R., Iaccarino G., 2005, "Immersed boundary methods", *Annual Review Fluid Mechanics* 37, 239-261

Okajima A., 1982, "Strouhal numbers of rectangular cylinders", *Journal of Fluid Mechanics* 123, 379-398

Tritton D. J. , 1959, "Experiments on the flow past a circular cylinder at low Reynolds number", Journal of Fluid Mechanics6, 547

William E. Lorensen, Harvey E., 1987, "Cline Marching Cubes: A high resolution 3D surface construction algorithm", *Computer Graphics* Vol. 21, Nr. 4, Juli 1987, 163-169